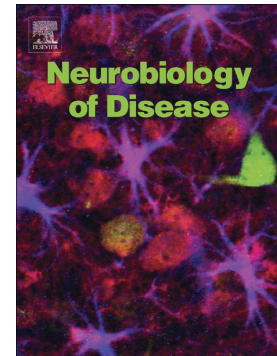


## Journal Pre-proof

Enhanced SPARCL1 expression in cancer stem cells improves preclinical modeling of glioblastoma by promoting both tumor infiltration and angiogenesis

Filippo Gagliardi, Ashwin Narayanan, Alberto Luigi Gallotti, Valentina Pieri, Stefania Mazzoleni, Manuela Cominelli, Sara Rezzola, Michela Corsini, Gianluca Brugnara, Luisa Altabella, Letterio Salvatore Politi, Marco Bacigaluppi, Andrea Falini, Antonella Castellano, Roberto Ronca, Pietro Luigi Poliani, Pietro Mortini, Rossella Galli



PII: S0969-9961(19)30380-8

DOI: <https://doi.org/10.1016/j.nbd.2019.104705>

Reference: YNBDI 104705

To appear in: *Neurobiology of Disease*

Received date: 31 July 2019

Revised date: 14 November 2019

Accepted date: 8 December 2019

Please cite this article as: F. Gagliardi, A. Narayanan, A.L. Gallotti, et al., Enhanced SPARCL1 expression in cancer stem cells improves preclinical modeling of glioblastoma by promoting both tumor infiltration and angiogenesis, *Neurobiology of Disease*(2019), <https://doi.org/10.1016/j.nbd.2019.104705>

This is a PDF file of an article that has undergone enhancements after acceptance, such as the addition of a cover page and metadata, and formatting for readability, but it is not yet the definitive version of record. This version will undergo additional copyediting, typesetting and review before it is published in its final form, but we are providing this version to give early visibility of the article. Please note that, during the production process, errors may be discovered which could affect the content, and all legal disclaimers that apply to the journal pertain.



*Submitted to Neurobiology of Disease*

**Enhanced *SPARCL1* expression in cancer stem cells improves preclinical modeling of glioblastoma by promoting both tumor infiltration and angiogenesis**

Filippo Gagliardi<sup>1,2</sup>, Ashwin Narayanan<sup>1§</sup>, Alberto Luigi Gallotti<sup>1,2§</sup>, Valentina Pieri<sup>1,5§</sup>, Stefania Mazzoleni<sup>1</sup>, Manuela Cominelli<sup>3</sup>, Sara Rezzola<sup>4</sup>, Michela Corsini<sup>4</sup>, Gianluca Brugnara<sup>5</sup>, Luisa Altabella<sup>5</sup>, Letterio Salvatore Politi<sup>5</sup>, Marco Bacigaluppi<sup>6</sup>, Andrea Falini<sup>5</sup>, Antonella Castellano<sup>5</sup>, Roberto Ronca<sup>4</sup>, Pietro Luigi Poliani<sup>3</sup>, Pietro Mortini<sup>2</sup>, and Rossella Galli<sup>1\*</sup>

<sup>1</sup> Neural Stem Cell Biology Unit, Division of Neuroscience, San Raffaele Scientific Institute, Via Olgettina 58, Milan, Italy, 20132;

<sup>2</sup> Dept. Neurosurgery and Gamma Knife Radiosurgery, San Raffaele Scientific Institute, Via Olgettina 60, Milan, Italy, 20132;

<sup>3</sup> Dept. Molecular and Translational Medicine, Pathology Unit, University of Brescia, Brescia, Italy, 25124;

<sup>4</sup> Dept. Molecular and Translational Medicine, Experimental Oncology and Immunology, University of Brescia, Brescia, Italy, 25124;

<sup>5</sup> Neuroradiology Unit and CERMAC, Vita-Salute San Raffaele University and San Raffaele Scientific Institute, Milan, Italy, 20132;

<sup>6</sup> Neuroimmunology Unit, Institute of Experimental Neurology (INSPE), Division of Neuroscience, San Raffaele Scientific Institute, Via Olgettina 58, Milan, Italy, 20132.

§: Shared co-authorship

\*: Corresponding author:

Rossella Galli, PhD

Neural Stem Cell Biology Unit Division of Neuroscience,  
San Raffaele Scientific Institute, Via Olgettina 58, 20132 Milan, Italy

Phone: +39 02 2643 4626

E-mail: galli.rossella@hsr.it

**Abstract**

Glioblastoma (GBM) is the most malignant brain tumor of adults and is characterized by extensive cell dissemination within the brain parenchyma and enhanced angiogenesis. Effective preclinical modeling of these key features suffers from several shortcomings. Aim of this study was to determine whether modulating the expression of extracellular matrix (ECM) modifiers in proneural (PN) and mesenchymal (MES) cancer stem cells (CSCs) and in conventional glioma cell lines (GCLs) might improve tumor invasion and vascularization. To this end, we selected secreted, acidic and rich in cysteine-like 1 (*SPARCLI*) as a potential mediator of ECM remodeling in GBM.

*SPARCLI* transcript and protein expression was assessed in PN and MES CSCs as well as GCLs, in their xenografts and in patient-derived specimens by qPCR, WB and IHC. *SPARCLI* expression was then enforced in both CSCs and GCLs by lentiviral-based transduction. The effect of *SPARCLI* gain-of-function on microvascular proliferation, microglia activation and advanced imaging features was tested in intracranial xenografts by IHC and MRI and validated by chorioallantoic membrane (CAM) assays.

*SPARCLI* expression significantly enhanced the infiltrative and neoangiogenic features of PN and MES CSC/GCL-induced tumors, with the concomitant activation of inflammatory responses associated with the tumor microenvironment, thus resulting in experimental GBMs that reproduced both the parenchymal infiltration and the increased microvascular density, typical of GBM.

Overall, these results indicate that *SPARCLI* overexpression might be instrumental for the generation of CSC-derived preclinical models of GBM in which the main pathognomonic hallmarks of GBMs are retrievable, making them suitable for effective preclinical testing of therapeutics.

## Introduction

Glioblastoma (GBM) is the deadliest brain tumor in adults and is characterized by extensive tumor cell dissemination within the brain that jeopardizes complete tumor removal, leading to refractoriness to treatment and invariable tumor recurrence (Olar and Aldape, 2014). With respect to other gliomas, GBM is characterized by extremely rapid infiltrative growth and enhanced angiogenesis.

Different molecular subtypes of GBM have been identified, with the genetic classification of GBM based on the IDH1 status being recently included into the histologic criteria-based diagnosis by the 2016 WHO classification of brain tumors (Louis et al., 2016). Very interestingly, a transcriptomics-based subtyping of GBM into proneural (PN), classical (CL) and mesenchymal (MES) subgroups has also been proposed (Phillips et al., 2006) (Verhaak et al., 2010) (Wang et al., 2017). The PN signature correlates with a slightly less aggressive disease and increased response to anti-angiogenic treatment in patients with IDH-wild-type GBM, whereas the MES subgroup is associated with enhanced angiogenesis, radio-resistance and poorer prognosis (Prados et al., 2015).

The availability of preclinical *in vivo* models reproducing both the histopathological and molecular features of the distinct transcriptional subgroups of GBM may provide a significant benefit to the field of neuro-oncology, as they can be exploited as valuable tools to dissect pathogenetic mechanisms and test patient-tailored treatments. Specifically, xenograft models, as those derived from the implantation of subgroup-specific cancer stem cells (CSCs) into immune-deficient mice, may be representative of the molecular complexity of GBM, while being easily attainable (Abounader, 2018).

CSCs can be isolated from GBM surgical specimens by the NeuroSphere Assay (NSA) and they can establish long-term renewing cell lines growing in suspension as neurospheres (Singh et al., 2003) (Galli et al., 2004) (Lee et al., 2006). Notably, the majority of CSC lines grown under the NSA conditions show a tendency to maintain or acquire molecular and pathological features typical of the PN transcriptional subgroup of GBMs, independent of the subgroup affiliation of the tumor of origin (Bhat et al., 2013) (Narayanan et al., 2018).

Upon intracranial transplantation, PN CSCs, cultured as neurospheres, are prone to give rise to highly infiltrative xenografts, which express canonical PN markers such as ASCL1, Olig2 and PDGFR $\alpha$  (Narayanan et al., 2018) and show a very limited extent of neoangiogenesis, as tumor cells preferentially coopt the preexisting brain vasculature, thus resembling low-grade rather than high-grade gliomas (Galli et al., 2004) (Narayanan et al., 2018) (Mazzoleni et al., 2010) (Eskilsson et al., 2016). On the contrary, MES CSCs (Narayanan et al., 2018) and serum-dependent traditional glioma cell lines (GCLs) (Galli et al., 2004) induce the generation of bulky, well-demarcated xenografts that express typical MES markers and are characterized by scarce tissue infiltration, exacerbated neoangiogenesis and contrast enhancement in magnetic resonance imaging (MRI).

To be noted, other modalities of CSC culturing, as those exploiting adherent conditions (Pollard et al., 2009), seem to better preserve the original subgroup identity of the GBM cell lines obtained (Xie et al., 2015). However, even under these *in vitro* conditions, adherent PN CSCs generate tumors that spread diffusely throughout the brain parenchyma, while MES xenografts grew expansively in nodular patterns, clearly demarcated from the normal parenchyma (Xie et al., 2015).

As such, either type of subgroup-specific preclinical model of GBM only partially reproduces the histopathological traits of the tumor, likely due to the downregulation of the expression of critical factors as a consequence of *in vitro* culturing.

To promote the neoangiogenic potential of PN CSC-derived xenografts and the infiltrative ability of MES CSC-derived tumors, thus making available more authentic and comprehensive rodent xenograft models of GBM than those currently available, we looked for mediators involved in extracellular matrix (ECM) remodeling, a process known to facilitate both angiogenesis and tumor infiltration. To this end, we focused our attention on a member of the secreted, acidic and rich in cysteine (SPARC) family of matricellular proteins, *i.e.* SPARC like 1 protein (SPARCL1), which we previously reported as being more highly expressed in more angiogenic EGFR<sup>neg</sup> CSCs than in less angiogenic EGFR<sup>pos</sup> CSCs (Mazzoleni et al., 2013). SPARCL1 is present in the ECM as a dynamically expressed non-structural protein, whose function is dependent on the type of tissue and on the presence of specific molecules, such as the aggrecanase ADAM Metallopeptidase With Thrombospondin Type 1 Motif 4 (ADAM15/4) that cleaves SPARCL1 into a peptide, termed SPARC-like fragment (SLF), which inhibits cell adhesion and stimulates cell migration (Weaver et al., 2011). Most remarkably, SPARCL1 is a critical component of a chemoattractant complex regulating the spreading of glioma cells within the brain and their interaction with neural stem cells (Qin et al., 2017).

Here we report that enforcing *SPARCL1* expression significantly enhances the infiltrative and neoangiogenic features of PN and MES CSC/GCLs-induced tumors, which are accompanied by increased inflammation, thus making the histopathological features of preclinical PN and MES GBMs more faithful of the ones observed in clinical samples than previous models.

## Results

### ***SPARCLI* expression correlates with EGFR expression in human GBM PN CSCs.**

Human EGFR<sup>neg</sup> and EGFR<sup>pos</sup> PN CSCs, classified based on EGFR protein expression, have been formerly shown to give rise to xenografts showing different level of angiogenesis, with EGFR<sup>neg</sup> PN CSCs being more angiogenic than EGFR<sup>pos</sup> (Mazzoleni et al., 2010) (**Supplementary Fig. S1**). To identify gene(s) potentially promoting angiogenesis, we took advantage of previously-generated microarray-based transcriptional data of EGFR<sup>neg</sup> and EGFR<sup>pos</sup> CSCs and compared, by supervised clustering analysis, the gene expression profile of EGFR<sup>neg</sup> CSC lines L0104, L0512 and L0125 with that of EGFR<sup>pos</sup> CSC lines L0605, L0306 and L0627 (Mazzoleni et al., 2010). Notably, 264 genes, ranked based on a log2 fold change >1 in expression with a  $p < 0.05$  significance, were differentially expressed between the two conditions (**Supplementary List S1**). In line with previous findings (Mazzoleni et al., 2010), one of the genes upregulated in EGFR<sup>neg</sup> CSCs vs. EGFR<sup>pos</sup> CSCs was *SPARCLI*. *SPARCLI* mRNA and protein were confirmed being significantly more highly expressed in EGFR<sup>neg</sup> CSCs than in EGFR<sup>pos</sup> CSC lines (**Fig. 1A-B**). Accordingly, *SPARCLI* expression was observed in a higher number of tumor cells in xenografts generated by the intracranial implantation of EGFR<sup>neg</sup> CSCs than in those induced by EGFR<sup>pos</sup> CSCs (**Fig. 1C**).

To assess whether *SPARCLI* expression held a clinical significance, we queried transcriptional information from the TCGA data set (Tumor Glioblastoma-TCGA-540-MAS5.0) of human GBM specimens, by using the R2 Genomics Analysis and Visualization Platform (<http://r2.amc.nl>). *SPARCLI* mRNA was expressed at very high levels in all the 4 transcriptional subgroups of GBM, thus implying that it might play a critical role in GBM (**Fig. 1D**). In agreement with R2-based transcriptional analysis, GBM specimens, molecularly classified by immunohistochemistry (IHC) for specific subgroup-restricted markers, showed similar *SPARCLI* protein expression in the two main molecular subgroups, *i.e.* proneural and mesenchymal ( $n=6$  and  $n=10$  patients for PN and MES, respectively) (**Fig. 1E**).

### ***SPARCLI* overexpression promotes extensive neoangiogenesis in PN CSC-derived intracranial xenografts.**

To understand whether *SPARCLI* might promote the acquisition of malignant features in GBM CSC-derived xenografts, we started by overexpressing *SPARCLI* in both EGFR<sup>pos</sup> (*i.e.* L0605 and L0306) and EGFR<sup>neg</sup> (*i.e.* L0512 and L0125) PN CSCs by lentiviral-mediated transduction. Both *SPARCLI* mRNA and protein were significantly more highly expressed in *SPARCLI*-transduced CSCs than in CSCs transduced with a control vector coding for GFP (mock) (**Supplementary Fig. S2A-B**).

In line with its main role in mediating interactions with ECM *in vivo*, *SPARCLI* overexpression in CSCs did not result in any significant difference in CSC morphology, long-term self-renewal,

proliferation rate, differentiation potential and invasive ability *in vitro* (data not shown). Likewise, we did not detect any significant alteration in signaling pathways associated with CSC physiology, e.g. AKT, ERK and mTOR (**Supplementary Fig. S2C**). However, the expression of ADAMTS4, the aggrecanase required for SPARCL1 cleavage into the active fragment, was slightly but significantly increased at the mRNA and protein level in *SPARCL1*-transduced CSCs *in vitro* (**Supplementary Fig. S2D-E**).

Next, we set out to test whether *SPARCL1* overexpression might elicit any effect *in vivo*. To this end, we transplanted orthotopically EGFR<sup>pos</sup> L0605 and EGFR<sup>neg</sup> L0512 CSCs transduced with either *GFP* or *SPARCL1* into nude mice ( $n=4$  animals/condition/CSC line for two independent experiments). In line with *in vitro* results, enhanced *SPARCL1* expression *in vivo*, which was comparable (**Supplementary Fig. S3**) to that seen in human GBM specimens (**Fig. 1E**), did not significantly affect either tumor growth or the overall survival of tumor-bearing mice (data not shown). Nonetheless, the extent of angiogenesis as assessed by IHC for CD31 was strongly increased in *SPARCL1*-transduced CSC-derived xenografts as compared to tumors derived from mock CSCs, in terms of both vessel number and area (vessel number and area per 20x field) (**Fig. 2A-B**) The increase was particularly evident in tumors derived from EGFR<sup>pos</sup> CSCs, whose basal level of *SPARCL1* and angiogenesis is low.

To understand whether the enlarged and tortuous vessels detected in *SPARCL1*-derived tumors were newly formed, immature vessels, we analyzed the degree of association of pericytes to endothelial cells in *GFP*- and *SPARCL1*-derived tumors. A tight lining of PDGFR $\beta$ <sup>pos</sup> pericytes was detected in most vessels retrieved in control xenografts, indicating that they were differentiated, mature and stable (**Fig. 2A, inset**). Conversely, reduced and discontinuous pericyte coverage was found in the majority of vessels in *SPARCL1*-transduced CSC-derived xenografts, implying that these vessels were immature and neoangiogenic (**Fig. 2A, insets**).

### ***SPARCL1*-overexpressing PN CSC-derived xenografts are endowed with angio-architectural patterns resembling those observed in patients.**

Since both vessel number and area were unevenly distributed within *SPARCL1*-transduced CSC-derived tumors, we analyzed the same parameters in three distinct anatomical compartments, classified as tumor core (TC), tumor periphery (TP), and tumor perilesional area (PA) (**Fig. 3A**). TP was defined as the peripheral area of the lesion, extending inside the tumor for 1 mm from the tumor border, whereas the PA was defined as the area of brain parenchyma surrounding the lesion, extending outside the tumor for 0.5 mm from the tumor border (**Fig. 3A**). The TC was identified as the remaining portion of the tumor (**Fig. 3A**).

Angiogenesis was significantly increased in all the three areas in *SPARCL1*-transduced CSC-derived tumors when compared to controls, and, in particular, higher vessel number and larger vessel

area were retrieved in the TP than in TC (**Fig. 3B-C** and **Supplementary Fig. S4A**). This pattern was reminiscent of GBM in patients, in which blood supply is typically supported by a peripheral ring-shaped active vasculature surrounding a central necrotic tumor core (Jain et al., 2007).

Another typical angiogenic feature of GBMs is the capability to recruit vessels from the surrounding brain parenchyma to sustain tumor growth. To assess whether this feature was present in tumors after overexpression of *SPARCL1*, we compared the angiogenic profile of the perilesional area in *GFP*- and *SPARCL1*-transduced CSC-derived xenografts. *SPARCL1*-overexpressing tumors displayed a significantly enhanced vessel recruitment in the PA as compared to controls (**Fig. 3B-C**). In agreement with these results, publicly available RNA sequencing data for anatomic structures isolated by laser microdissection in a collection of 122 samples from 10 human GBMs (Ivy Glioblastoma Atlas Project, Ivy Gap; <http://glioblastoma.alleninstitute.org>) indicated that *SPARCL1* expression was significantly higher in the infiltrating part and in the leading edge of the tumor than in the rest of the tumor (**Fig. 3D**).

To understand whether *SPARCL1* expression was directly regulating neoangiogenesis in CSC-derived xenografts, we performed different angiogenic-specific assays *in vitro* and *ex-vivo*. Firstly, we assessed the expression of known angiogenic factors in CSCs overexpressing *GFP* or *SPARCL1* by qPCR. In line with previous *in vitro* analyses, no consistent difference was detected in the expression of *HIF1 $\alpha$* , *VEGF* and *POSTN*, when assessed in CSC cultures after *SPARCL1* overexpression (**Supplementary Fig. S4B**).

Next, we evaluated the sprouting and proliferation of human umbilical vein endothelial cells (HUVECs) after stimulation with either mitogen-supplemented or mitogen-free conditioned media (CM) from CSCs overexpressing *GFP* or *SPARCL1*. No significant differences in terms of spheroid formation and proliferation were detected with any CM collected from either *GFP*- or *SPARCL1*-transduced CSCs (data not shown).

As such, we hypothesized that a more complex microenvironment than that provided by two-dimension endothelial cell cultures could be required to dissect the effect of *SPARCL1* on angiogenesis. To this end, we exploited the *ex-vivo* three-dimension chick embryo chorioallantoic membrane (CAM) assay. Several CAMs were exposed to mitogen-supplemented CM and only the CM from *SPARCL1*-overexpressing EGFR<sup>neg</sup> CSC was able to induce a significant angiogenic response (**Fig. 3E**). Since the continuous production of *SPARCL1*, whose lability *in vitro* has been previously documented (Weaver et al., 2011), together with the direct contact of CSCs with the microenvironment might be necessary for the full pro-angiogenic effect to take place, we assessed the direct proangiogenic effect of *GFP*- and *SPARCL1*-overexpressing CSCs by placing them on top of the CAM. Under these conditions, a statistically relevant promotion in vessel outgrowth was observed with all *SPARCL1*-transduced CSC lines as compared to controls (**Fig. 3E**).

***SPARCLI* induces a significant recruitment of activated microglia that parallels the enhancement in angiogenesis.**

*SPARCLI* role in angiogenesis may also be mediated indirectly by the interaction with the host-derived microenvironment. To assess the contribution of microglia/macrophages in *GFP*- and *SPARCLI*-transduced CSC-derived xenografts, IHC was performed by antibodies directed against Iba1, a known molecular marker of both resting and activated microglia as well as of macrophages, and the number of microglia/macrophages quantified in the three distinct tumor compartments (**Fig. 4A**).

As compared to controls, *SPARCLI*-transduced CSC-derived tumors showed increased numbers of Iba1<sup>POS</sup> cells (**Fig. 4B and Supplementary Fig. S5A**). In line with the compartmentalized vessel analysis (**Fig. 3**), xenografts generated from *SPARCLI*-transduced CSCs showed a significant increase in the number of microglial cells located in the TP as compared to the TC (**Fig. 4B-C**).

When functionally activated, microglial cells assume a round, amoeboid-like shape. A significant increase in amoeboid Iba1<sup>POS</sup> cells was retrieved in xenografts generated by *SPARCLI*-transduced CSCs as compared to controls, thus suggesting that there might be an increase in microglia activation upon *SPARCLI* overexpression (**Fig. 4D**).

We next took advantage of the previously described bioinformatics tool R2 to explore the relationship between *SPARCLI* expression and the nature of the immune infiltrate (Zhao et al., 2018). In line with *in vivo* results, Pearson correlation analysis on the TCGA GBM data set indicated a positive correlation between the expression of *SPARCLI* in patients' GBMs and that of total tumor-associated macrophages/microglia markers such as *Iba1* (*AIF1*) (r-value=0.301, p-value=8.4e-13) and *CD11b* (*ITGAM*) (r-value=0.237, p-value=2.8e-10) (**Fig. 4E**). A significant positive correlation was found for the M2 macrophage markers *CD163* (r-value=0.134, p-value=1.7e-03) and a positive trend for *iNOS* (*NOS2*) (r-value=0.055, p-value=0.20) (**Fig. 4E**), while no correlation was found with the M1-associated markers *H1A-DR* and *CD11c* (*ITGAX*) (data not shown). Similar findings were retrieved when the smaller-sized Ivy Gap dataset was used, with significant correlation observed for *Iba1* (**Supplementary Fig. S6**). Therefore, a global increase in tumor-associated macrophages might be involved in mediating the *SPARCLI*-dependent angiogenic phenotype, thus again reproducing a pattern similar to that observed in highly malignant GBMs.

When correlation analysis was performed by taking advantage of expression data of the selected anatomic areas reported in the Ivy Gap dataset, a positive correlation was found between *SPARCLI* and *CD163* (r-value=0.628) and a positive trend with the remaining genes in the cellular portion of the tumor (**Supplementary Fig. S6**). On the contrary, anticorrelation was detected between *SPARCLI* and *Iba1* (r-value=-0.506), *CD163* (r-value=-0.64) and *CD11c* (r-value=-0.413) in the infiltrative region of the tumor (**Supplementary Fig. S6**). Correlation in the remaining tumor areas was not significant (not shown).

### **Advanced MR imaging identifies increased angiogenesis and infiltration in SPARCL1-overexpressing PN CSC-derived xenografts.**

Intracranial xenografts generated by PN CSCs do not enhance at MRI after contrast agent administration (Mazzoleni et al., 2010). Indeed, PN CSCs co-opt the pre-existing vasculature and do not alter the blood-brain barrier (BBB), as they give rise to highly infiltrative tumors, which are characterized by hyperintensity in T2-weighted images and hypointensity in T1-weighted images (Di Tomaso et al., 2010).

To assess if SPARCL1-dependent pro-angiogenic effect could result in MRI-detectable changes in microvascular density and/or BBB permeability, anatomic T1-weighted/T2-weighted, dynamic-contrast enhancement (DCE) and diffusion tensor imaging (DTI) analyses were performed on Rowett Nude female rats transplanted with *GFP*- and *SPARCL1*-overexpressing L0605 CSCs by a 7-Tesla small animal-dedicated MRI equipment.

In agreement with findings in mice, vessel number, vessel area and Iba<sup>pos</sup> cells were increased in *SPARCL1*-overexpressing CSC-derived tumors in rats (**Fig. 5A** and **Supplementary Fig. S5B**).

An increase in post-gadolinium enhancement by T1-weighted MRI (**Fig. 5B**) and in tumor vascularity through quantification of plasma volume ( $v_p$ ) by perfusion-weighted DCE analysis (**Fig. 5C**) was observed in *SPARCL1*-overexpressing tumors (**Supplementary Table 1**), suggesting the occurrence of both BBB disruption and increased vessel density.

In addition, the tumor volume segmented on T2-weighted images in *SPARCL1*-overexpressing tumors was smaller than the tumor volume segmented on diffusion tensor-derived pure isotropy ( $p$ ) maps (**Fig. 5D** and **Supplementary Table 1**), implying that *SPARCL1* expression might promote extensive infiltration of single tumor cells within the brain parenchyma.

### **SPARCL1 expression in glioma cell lines (GCLs) and mesenchymal CSCs enhances neoangiogenesis and induce invasion.**

Up to this point, we demonstrated that increasing *SPARCL1* expression in PN CSCs strongly promotes their neoangiogenic potential and parenchymal invasion, thus significantly contributing to the improvement of high-grade glioma features in PN CSC-derived preclinical models. Next, we set out to test whether *SPARCL1* overexpression might elicit the same effect in GBM cells endowed with mesenchymal features. To this end, we first took advantage of traditional glioma cell lines (GCLs), such as U87 and U373, and then validated the findings in a NSA-grown MES CSC line, *i.e.* L1312, which is known to retain a mesenchymal phenotype (Narayanan et al., 2018). Of note, GCLs and MES CSCs show a poorly invasive growth pattern *in vivo*, thus not reproducing this critical pathognomonic feature of GBM. On the contrary, they both give rise to tumors with enhanced neoangiogenesis (Galli et al., 2004) (Narayanan et al., 2018).

Although patients' MES GBMs express significant levels of *SPARCL1* transcript and protein (**Fig. 1**), GCLs and MES CSCs did not, when compared to PN CSCs (**Supplementary Fig. S7A-B**), implying that *in vitro* culturing might have selected for cell clones that did not express *SPARCL1* and suggesting that the regulation of neoangiogenesis in MES cells may be primarily *SPARCL1*-independent. Nonetheless, when *SPARCL1* was overexpressed in these cell lines (**Supplementary Fig. S7C-D**), we observed a significant further increase in vessel density and area as compared to mock cells, as well as the presence of immature vessels with scarce pericyte coverage, as previously detected in *SPARCL1*-transduced PN CSC-derived xenografts (**Fig. 6A-B**). Likewise, enhanced infiltration by tumor-associated macrophages/microglial cells was also retrieved, in particular at the TP, in xenografts from *SPARCL1*-overexpressing GCLs (**Fig. 6C-D**).

*SPARCL1* overexpression in non-infiltrative GCLs and MES CSCs also significantly promoted *in vivo* invasive ability, as shown by modifications occurring at the tumor-parenchyma boundary, with the well-delimited tumor border typical of GCLs and MES CSCs being interrupted by clusters of tumor cells departing from the main tumor mass (**Fig. 6E**).

#### **SPARCL1-induced neoangiogenesis is not primarily mediated by microglia.**

To understand whether *SPARCL1* acted directly or indirectly to promote angiogenesis by interacting with microglia, we treated mice transplanted with *GFP*- or *SPARCL1*-overexpressing U87 GCLs with two different CSFR1 inhibitors, namely GW2580 and PLX3397. The GW2580 inhibitor is a highly specific CSFR1 inhibitor able to induce 30% depletion of microglia cells and to reduce their proliferation (Olmos-Alonso et al., 2016). On the contrary, PLX3397 inhibitor is slightly less specific, as it inhibits also Flt3 and c-Kit receptors on vessels, but is highly effective in microglia depletion (60-90% efficiency of microglia ablation) (Peranzoni et al., 2018).

Mice transplanted with *GFP*-transduced U87 cells were fed with a control chow (*GFP* CTR;  $n=4$ ), while those transplanted with *SPARCL1*-transduced U87 cells were treated with *a*) a control chow (*SPARCL1* CTR;  $n=4$ ), *b*) a GW2580-containing chow (*SPARCL1* GW2580;  $n=4$ ) and *c*) a PLX3397-containing chow (*SPARCL1* PLX3397;  $n=4$ ).

No treatment-related changes in tumor volume were detected (data not shown). In line with previous reports, the frequency of Iba1<sup>POS</sup> cells was significantly reduced after treatment with either of the inhibitors (**Fig. 7A-B**). However, the number of vessels and their area were decreased to a much lower extent, suggesting that microglia may only partially mediate the *SPARCL1*-induced increase in angiogenesis (**Fig. 7A-B**).

## Discussion

Only a small set of preclinically-tested drugs have been shown to successfully enter clinical trialing, likely due to limitations in the preclinical pipeline of cancer models (Floc'h et al., 2018). Conventional cell line-derived xenografts showed scarce resemblance with the original tumors, in particular in terms of tumor heterogeneity. Likewise, patient-derived xenografts demonstrated limited value in anticipating clinical trial response at the population level (Floc'h et al., 2018).

The translational relevance of preclinical *in vivo* models concerns also GBM modeling. GBM is a highly heterogenous cancer, which comprises cells with distinct molecular profiles. Indeed, a recent study reported that cells belonging to 4 main different cell lineage related-states may be identified by single cell-RNA seq in a collection of GBM patients (Nefitel et al., 2019). These 4 states again recapitulated the 3 main molecular subgroups, *i.e.* proneural, classical and mesenchymal. Most notably, although each GBM sample did comprise cells belonging to all 4 different fates, a predominant cell population could be retrieved, indicating that most GBM samples could be safely affiliated to a specific subgroup. Due to the complexity and heterogeneity of the disease, no preclinical model is currently available that mimics all the relevant histopathological and molecular features of the tumor (Abounader, 2018).

Others and we reported that PN GBM CSCs give rise to intracranial tumors that tend to recapitulate features of low-grade gliomas, as they are characterized by high tissue infiltration and very limited neoangiogenesis (Bhat et al., 2013) (Narayanan et al., 2018). Since enhanced angiogenesis is a major GBM hallmark, preclinical models that lack this ability may suffer from severe limitations in predicting therapy responsiveness. Conversely, mesenchymal GBM xenografts, as those promoted by transplantation of conventional GCLs and MES CSCs, while being endowed with extensive microvascular proliferation, do not show any sign of parenchymal infiltration (Narayanan et al., 2018). As such, although PN and MES CSCs reproduce many histological features of either subgroup, effective preclinical modeling reproducing all GBM characteristics has not been achieved to date.

Here we report that by modulating the expression of a single ECM interactor, *i.e.* *SPARCL1*, we promoted the acquisition of neoangiogenic traits in PN CSC-derived xenografts and the enhancement of infiltration in GCL/MES CSC-derived tumors.

*SPARCL1* is an antiadhesive protein that exert tumorigenic or anti-tumorigenic activity depending on the tumor type. In colorectal cancer, the expression of *SPARCL1* is considered a reliable marker for early diagnosis as well as a prognostic factor in patients (Zhang et al., 2011). Conversely, in pancreatic cancer *SPARCL1* shows anti-invasive activity and is lowly expressed in metastasis (Esposito et al., 2007).

Concerning gliomas, in line with our findings, *SPARCL1* protein expression was reported to increase concomitant with tumor grade (Turtoi et al., 2012). Moreover, *SPARCL1* is a required mediator of the complex responsible for the invasion-promoting effect of subventricular zone progenitors during infiltration of glioma cells in the brain, thus reinforcing its role as pro-invasive factor (Qin et al., 2017).

SPARC, also referred to as osteonectin or BM-40, is the prototypical member of the large family of SPARC matricellular proteins (Jones and Bouvier, 2014). Interestingly, the increase in tumor infiltration that we observed following *SPARCL1* overexpression in GCLs/MES CSCs is in line with previous findings demonstrating that enhancing SPARC expression in U87 cells result in tumor cells invading the brain as tumor satellites (Schultz et al., 2002) (Thomas et al., 2010). However, as opposed to the reported SPARC antiproliferative activity (Schultz et al., 2002) (Thomas et al., 2010), we did not observe any significant inhibitory effect of SPARCL1 on tumor growth, thus suggesting that SPARC and SPARCL1 act differently in regulating glioma pathogenesis. Accordingly, whereas SPARC suppresses glioma vascularization (Yunker et al., 2006), here we demonstrate that SPARCL1 enhanced this feature in both CSC- and GCL-derived xenografts. As such, SPARCL1 seems to serve as a better molecular candidate than SPARC to promote the acquisition of GBM infiltrative and angiogenic properties, while not affecting tumor growth.

Under hypoxia, pseudopalisading regions in GBM activate ECM proteins (*e.g.* matrix metalloproteinases, protease-activated receptors, etc.) that induce GBM cells to migrate away from vessels (Brat et al., 2004). As the tumor cells retract, they secrete proangiogenic factors that stimulate neoangiogenesis and outward expansion of tumor towards the newly formed vessels (Rong et al., 2006). As such, also the increase in vessel recruitment at the perilesional tumor border, where tumor cells are actively infiltrating as single cells, might be directly mediated by SPARCL1. Advanced MRI analysis seems to corroborate these observations, as the higher tumor volume on diffusion tensor-derived isotropic maps than in T2-weighted images may reflect a more invasive tumor phenotype of *SPARCL1*-overexpressing tumors than controls (Price et al., 2017).

GBM are characterized by a high degree of infiltration by immune cells that actively participate to ECM remodeling. Our findings suggest that SPARCL1 expression in CSC-derived xenografts promotes the increase of innate immunity cells, such as microglia and pro-tumorigenic M2 macrophages, that is another qualifying feature of highly malignant gliomas. In fact, data obtained after depletion of microglia reinforce the notion that *SPARCL1* is the main and direct mediator of tumor neovascularization and that the role of microglia is mostly ancillary.

In summary, the above-described GBM mouse models are endowed with relevant characteristics that should facilitate their exploitation by researchers studying GBM. To date, the lack of any significant clinical impact of GBM molecular subtyping has diminished the importance of studies focused on investigating GBM molecular subtypes. The availability of CSC-derived mouse models

that recapitulate simultaneously the molecular features of GBMs (*e.g.* proneural and mesenchymal CSCs) and their major histopathological characteristics (tissue invasion, angiogenesis and tumor-immune host microenvironment cross-talk) will provide a valuable and unprecedented experimental tool to be exploited for a reliable preclinical testing that takes into account the molecular subgroup affiliation of GBM.

Journal Pre-proof

## Material and methods

### *In vitro* culture of GBM CSCs and GCLs

PN and MES GBM CSCs, established at the Neural Stem Cell Biology Unit, San Raffaele Scientific Institute, Milan, Italy and validated in (Narayanan et al., 2018) and (Mazzoleni et al., 2010), were cultured under the conditions of the NeuroSphere Assay (NSA) (Galli et al., 2004). GCL lines were grown in DMEM containing 10% fetal bovine serum (FBS) (Galli et al., 2004).

### Microarray-Based Gene Expression Profiling

Total RNA was isolated from CSCs using the RNeasy Mini Kit (Qiagen, Chatsworth, CA, USA). Biotinylated cRNA probes were synthesized using the GeneChip Whole Transcript Sense Target Labeling Assay Kit (Affymetrix) and then hybridized for 17hr at 45°C on GeneChip® Human Gene 1.0 ST Array (Affymetrix). Details of bioinformatics analysis are provided as Supplementary Methods.

### Quantitative real-time PCR

One µg of total RNA was reverse-transcribed by using first strand synthesis kit Superscript III RNaseH<sup>-</sup> Reverse Transcriptase (Invitrogen, Carlsbad, CA) and OligodT primers. Quantitative real-time PCR was performed by the IQ SybrGreen<sup>®</sup> technology (Biorad, Hercules, CA, USA) following manufacturer's instructions. β-actin was used as housekeeping gene. Human-specific primers for *SPARCL1* were purchased from Sigma (KODqStart™ Primers). Data analysis was performed by the  $\Delta\Delta C_t$  method.

### Bright-field immunohistochemistry

The retrospective study on human samples was conducted in compliance with the Declaration of Helsinki and with policies approved by the Ethics Board of Spedali Civili di Brescia, University of Brescia. For retrospective and exclusively observational study on archival material obtained for diagnostic purpose, patient consent was not needed.

Two µm sections were cut from paraffin blocks containing subgroup-classified human GBM samples as well as brains from mice transplanted with GBM CSCs/GCLs. Primary antibodies used for the stainings were: goat anti-PECAM-1 (CD31) (M-20) (Santacruz Biotechnology), rabbit anti-Iba1 (Wako Chemical GmbH), goat anti-PDGFRβ (RD Systems) and goat anti-SPARCL1 (RD Systems). Sections were then incubated with the secondary antibody (ChemMATE Envision Rabbit/Mouse, Dako Cytomation). Vessel number and area were quantified by the software ImageJ (<https://imagej.nih.gov/ij/>).

### Western Blotting

Lysates from CSCs and GCLs were homogenized in 10x volume of RIPA lysis buffer. Proteins were separated by electrophoresis on 8-10% polyacrilamide (Sigma-Aldrich, St. Louis, MO) gels and transferred onto trans-blot nitrocellulose membranes (Amersham). The primary antibodies/antisera used were goat anti-SPARCL1 (RD Systems), rabbit anti-ADAMTS4 (Novus Biological) and mouse anti-calnexin (Genetex). Secondary antibodies were horseradish peroxidase-conjugated (Amersham). Reactive proteins were visualized using LiteBlot (Euroclone, Padriciano, Italy) and exposure to x-ray film (BioMax MR; Kodak, Rochester, NY).

### Generation of lentiviral vectors for gene expression

The cDNA for human *SPARCL1* (Upstate, Lake Placid, NY, USA) was cloned into the pC.sin.cPPT.PGK.GFP.WPRE11 monocistronic transfer lentiviral vector (LV) in place of the GFP sequence. The pCCL.sin.cPPT.PGK.GFP.WPRE11 vector was used as mock condition. GBM CSCs and GCLs were transduced with  $1 \times 10^7$  TU/ml of LVs for 16 hours.

### Orthotopic implantation of GBM cells

All animal experiments were approved by the Institutional Ethics Review Board at San Raffaele Scientific Institute and by the Italian Ministry of Health and performed in accordance with the guidelines of the International Animal Care and Use Committee.

Two  $\times 10^5$  CSCs/GCLs were suspended in 2  $\mu$ l of DMEM supplemented with DNase and delivered into the right striatum of 8-week old *nu/nu* female mice by stereotactic injection with a micro-syringe (Hamilton). For MRI studies,  $1 \times 10^6$  GBM CSCs were suspended in 5  $\mu$ l of DMEM and injected into the right striatum of 4-week old Rottweil Nude female rats.

### Chorioallantoic membrane (CAM) assay

Alginate beads (5  $\mu$ L) containing GBM CSCs ( $3 \times 10^4$  cells/embryo) were placed on top of the chicken embryo CAM of fertilized White Leghorn chicken eggs at day 11 of incubation (6 to 8 eggs per experimental group) (Ribatti et al., 1997). After 72 hours, blood vessels converging toward the implant were counted under a stereomicroscope (STEMI-SR, x2/0.12; Zeiss) at 20X magnification.

### MRI acquisition and analysis

MRI was performed on a small animal-dedicated 7T scanner (30/70 BioSpec; Bruker, Ettlingen, Germany). The animal protocol included high resolution T2 and T1 sequences as well as advanced perfusion and diffusion MRI. Dynamic contrast-enhanced (DCE) perfusion MR imaging was performed by using a dynamic gradient-echo T1-weighted sequence during the injection of

gadobutrol (Gadovist; Bayer Schering Pharma, Germany). Diffusion Tensor Imaging (DTI) was performed using a two-shell acquisition. Details of the MRI sequences and analysis are provided as Supplementary Methods.

### **Microglia depletion by CSFR1 pharmacological inhibition**

For treatment with GW2580, mice were fed with 0.1% GW2580 (Selleckchem) assembled to chow (D17121401i, Research Diets) or vehicle in control chow (D1001i, Research Diets) (Olmos-Alonso et al., 2016), whereas for treatment with PLX 3397, they were fed with pexidartinib (Selleckchem) assembled to chow (290mg/kg, D15082602i, Research Diets) or the same control chow as above.

Mice to be transplanted with the different U87 GCL populations started being fed with control or GW2580-containing chow 10 days before transplantation and with PLX3397-containing chow 7 days before transplantation. Treatment continued for 14 days after transplantation.

Three  $\times 10^5$  U87 GCLs were suspended in 3 $\mu$ l of DMEM supplemented with DNase and delivered into the right striatum of 8-week old NSG female mice by stereotactic injection with a micro-syringe (Hamilton). Tumor development was monitored by T2-weighted MRI and mice were sacrificed 2 weeks after transplant.

### **Statistics**

For experiments involving patients' samples or *in vitro* CSC/GCL cultures,  $n$  represents the number of single patient-derived samples and CSC lines. For experiments involving transplanted CSC/GCL lines,  $n$  represents the number of individual animals that were transplanted with a single cell line.

Results for continuous variables were expressed as mean  $\pm$  standard error mean (s.e.m.). Two-group comparisons were performed with the independent samples' one-tailed Student  $t$  test. P values  $<0.05$  were considered statistically significant. \*:  $p<0.05$ ; \*\*:  $p<0.01$ ; \*\*\*:  $p<0.005$ ; \*\*\*\*:  $p<0.001$ .

**Competing interests**

The authors declare no potential conflicts of interest.

**Funding:**

This study was supported by Associazione Italiana Ricerca sul Cancro (AIRC) grant IG12924 to R.G.

**Authors' contributions**

Conceptualization, F.G. and R.G.; Methodology, F.G., R.R., M. B., A.C., and R.G.; Investigation, F.G., A.N., A.L.G, V.P., S.M., M.C., S.R., Mi.C., G.B., L.A., L.S.P., M. B., A.C., P.L.P., R.G.; Formal Analysis, F.G., A.N., A.L.G, V.P., R.R., R.G.; Resources A.F, P.M.; Writing – Original Draft, F. G. and R.G.; Writing – Review & Editing, F. G., A.N., A.L.G., V.P., R.R., A.C., P.L.P., R.G.; Visualization, R.G.; Supervision, R.G.; Project Administration, R.G.; Funding Acquisition, R.G.

**Acknowledgements**

We thank Tamara Canu for the expert assistance in the small animal 7 Tesla-based MRI acquisition carried out at the Preclinical Imaging Facility of the Experimental Imaging Center, established at the San Raffaele Scientific Institute and the Vita-Salute San Raffaele University.

## References

- Abounader, R., 2018. A new practical and versatile mouse model of proneural glioblastoma. *Neuro Oncol.* 20, 299-301.
- Bhat, K. P., et al., 2013. Mesenchymal differentiation mediated by NF-kappaB promotes radiation resistance in glioblastoma. *Cancer Cell.* 24, 331-46.
- Brat, D. J., et al., 2004. Pseudopalisades in glioblastoma are hypoxic, express extracellular matrix proteases, and are formed by an actively migrating cell population. *Cancer Res.* 64, 920-7.
- Di Tomaso, T., et al., 2010. Immunobiological characterization of cancer stem cells isolated from glioblastoma patients. *Clin Cancer Res.* 16, 800-13.
- Eskilsson, E., et al., 2016. EGFRvIII mutations can emerge as late and heterogenous events in glioblastoma development and promote angiogenesis through Src activation. *Neuro Oncol.* 18, 1644-1655.
- Esposito, I., et al., 2007. Tumor-suppressor function of SPARC-like protein 1/170 in pancreatic cancer. *Neoplasia.* 9, 8-17.
- Floch, N., et al., 2018. Optimizing the design of population-based patient-derived tumor xenograft studies to better predict clinical response. *Dis Model Mech.* 11.
- Galli, R., et al., 2004. Isolation and Characterization of Tumorigenic, Stem-like Neural Precursors from Human Glioblastoma. *Cancer Res.* 64, 7011-21.
- Jain, R. K., et al., 2007. Angiogenesis in brain tumours. *Nat Rev Neurosci.* 8, 610-22.
- Jones, E. V., Bouvier, D. S., 2014. Astrocyte-secreted extracellular proteins in CNS remodelling during development and disease. *Neural Plast.* 2014, 321209.
- Lee, J., et al., 2006. Tumor stem cells derived from glioblastomas cultured in bFGF and EGF more closely mirror the phenotype and genotype of primary tumors than do serum-cultured cell lines. *Cancer Cell.* 9, 391-403.
- Louis, D. N., et al., 2016. The 2016 World Health Organization Classification of Tumors of the Central Nervous System: a summary. *Acta Neuropathol.* 131, 803-20.
- Mazzoleni, S., et al., 2010. Epidermal growth factor receptor expression identifies functionally and molecularly distinct tumor-initiating cells in human glioblastoma multiforme and is required for gliomagenesis. *Cancer Res.* 70, 7500-13.
- Narayanan, A., et al., 2018. The proneural gene ASCL1 governs the transcriptional subgroup affiliation in glioblastoma stem cells by directly repressing the mesenchymal gene NDRG1. *Cell Death Differ.*
- Neftel, C., et al., 2019. An Integrative Model of Cellular States, Plasticity, and Genetics for Glioblastoma. *Cell.* 178, 835-849 e21.
- Olar, A., Aldape, K. D., 2014. Using the molecular classification of glioblastoma to inform personalized treatment. *J Pathol.* 232, 165-77.
- Olmos-Alonso, A., et al., 2016. Pharmacological targeting of CSF1R inhibits microglial proliferation and prevents the progression of Alzheimer's-like pathology. *Brain.* 139, 891-907.
- Peranzoni, E., et al., 2018. Macrophages impede CD8 T cells from reaching tumor cells and limit the efficacy of anti-PD-1 treatment. *Proc Natl Acad Sci U S A.* 115, E4041-E4050.
- Phillips, H. S., et al., 2006. Molecular subclasses of high-grade glioma predict prognosis, delineate a pattern of disease progression, and resemble stages in neurogenesis. *Cancer Cell.* 9, 157-73.

- Pollard, S. M., et al., 2009. Glioma stem cell lines expanded in adherent culture have tumor-specific phenotypes and are suitable for chemical and genetic screens. *Cell Stem Cell.* 4, 568-80.
- Prados, M. D., et al., 2015. Toward precision medicine in glioblastoma: the promise and the challenges. *Neuro Oncol.* 17, 1051-63.
- Price, S. J., et al., 2017. Less Invasive Phenotype Found in Isocitrate Dehydrogenase-mutated Glioblastomas than in Isocitrate Dehydrogenase Wild-Type Glioblastomas: A Diffusion-Tensor Imaging Study. *Radiology.* 283, 215-221.
- Qin, E. Y., et al., 2017. Neural Precursor-Derived Pleiotrophin Mediates Subventricular Zone Invasion by Glioma. *Cell.* 170, 845-859 e19.
- Ribatti, D., et al., 1997. New model for the study of angiogenesis and antiangiogenesis in the chick embryo chorioallantoic membrane: the gelatin sponge/chorioallantoic membrane assay. *J Vasc Res.* 34, 455-63.
- Rong, Y., et al., 2006. 'Pseudopalisading' necrosis in glioblastoma: a familiar morphologic feature that links vascular pathology, hypoxia, and angiogenesis. *J Neuropathol Exp Neurol.* 65, 529-39.
- Schultz, C., et al., 2002. Secreted protein acidic and rich in cysteine promotes glioma invasion and delays tumor growth in vivo. *Cancer Res.* 62, 6270-7.
- Singh, S. K., et al., 2003. Identification of a cancer stem cell in human brain tumors. *Cancer Res.* 63, 5821-8.
- Thomas, S. L., et al., 2010. PTEN augments SPARC suppression of proliferation and inhibits SPARC-induced migration by suppressing SHC-RAF-ERK and AK1 signaling. *Neuro Oncol.* 12, 941-55.
- Turtoi, A., et al., 2012. Sparc-like protein 1 is a new marker of human glioma progression. *J Proteome Res.* 11, 5011-21.
- Verhaak, R. G., et al., 2010. Integrated genomic analysis identifies clinically relevant subtypes of glioblastoma characterized by abnormalities in PTEN, IDH1, EGFR, and NF1. *Cancer Cell.* 17, 98-110.
- Wang, Q., et al., 2017. Tumor Evolution of Glioma-Intrinsic Gene Expression Subtypes Associates with Immunological Changes in the Microenvironment. *Cancer Cell.* 32, 42-56 e6.
- Weaver, M., et al., 2011. Proteolysis of the matricellular protein hevin by matrix metalloproteinase-3 produces a SPARC-like fragment (SLF) associated with neovasculature in a murine glioma model. *J Cell Biochem.* 112, 3633-3642.
- Xie, Y., et al., 2015. The Human Glioblastoma Cell Culture Resource: Validated Cell Models Representing All Molecular Subtypes. *EBioMedicine.* 2, 1351-63.
- Yunker, C. K., et al., 2008. SPARC-induced increase in glioma matrix and decrease in vascularity are associated with reduced VEGF expression and secretion. *Int J Cancer.* 122, 2735-43.
- Zhang, H., et al., 2011. SPARCL1: a potential molecule associated with tumor diagnosis, progression and prognosis of colorectal cancer. *Tumour Biol.* 32, 1225-31.
- Zhao, S. J., et al., 2018. SPARCL1 suppresses osteosarcoma metastasis and recruits macrophages by activation of canonical WNT/beta-catenin signaling through stabilization of the WNT-receptor complex. *Oncogene.* 37, 1049-1061.

## Figure Legends

### Fig. 1 - *SPARCL1* expression correlates with EGFR in human GBM PN CSCs.

(A-B) *SPARCL1* mRNA and protein are upregulated in EGFR<sup>neg</sup> vs. EGFR<sup>pos</sup> PN CSC lines ( $n=5$  and  $n=4$  for qRT-PCR on EGFR<sup>pos</sup> and EGFR<sup>neg</sup> PN CSC lines, respectively;  $n=2$  for WB on EGFR<sup>pos</sup> and EGFR<sup>neg</sup> PN CSC lines).

(C) *SPARCL1* expression is higher in EGFR<sup>neg</sup> than in EGFR<sup>pos</sup> CSC-derived tumors (IHC) (*SPARCL1*, brown) ( $n=3$  for each type). Scale bar: 50 $\mu$ m.

(D) *SPARCL1* is highly expressed in human PN, neural, classical and MES GBM subgroups as reported in dataset Tumor Glioblastoma-TCGA-540-MAS5.0.

(E) *SPARCL1* protein expression by IHC is retrieved with a similar pattern in GBM specimens classified as PN and MES ( $n=6$  and  $n=10$  patients for PN and MES, respectively). Scale bar: 50 $\mu$ m.

### Fig. 2 - *SPARCL1* overexpression promotes extensive neoangiogenesis in PN CSC-derived intracranial xenografts.

(A) *SPARCL1* overexpression promotes angiogenesis in both EGFR<sup>neg</sup> and EGFR<sup>pos</sup> CSC-derived xenografts ( $n=4$  and  $n=9$  mice for EGFR<sup>neg</sup> and EGFR<sup>pos</sup> CSCs/condition, respectively) (H&E; CD31 staining for vessels, brown; PDGFR $\beta$  staining for pericytes, brown). Scale bar: 100 $\mu$ m.

(B) Both vessel density and area are significantly increased by *SPARCL1* overexpression over time (400x field).

### Fig. 3 - *SPARCL1*-overexpressing PN CSC-derived xenografts are endowed with angiogenic architectural patterns resembling those observed in patients.

(A) Compartmentalization of CSC-derived tumors into three main regions. TC: tumor core; TP: tumor periphery; PA: perilesional area. Upper panel: staining for human EGFR (brown); lower panel: staining for CD31 (brown).

(B-C) Increased angiogenesis in the TP and significantly enhanced vessel recruitment in the PA after *SPARCL1* overexpression. Scale bar: 100 $\mu$ m.

(D) *SPARCL1* expression is significantly higher in the tumor infiltrating part, in the leading edge and in areas characterized by microvascular proliferation.

(E) *SPARCL1*-overexpressing CSCs exert a significant pro-angiogenic effect when seeded in direct contact with the membrane in the CAM assay than the CM from the same cells. Increased vessel density is indicated by arrows.

### Fig. 4 - *SPARCL1* induces a significant increase in activated microglia that parallels the enhancement in angiogenesis.

- (A) Compartmentalization of CSC-derived tumors into three main regions. Upper panel: staining for human EGFR; lower panel: staining for the microglial marker Iba1 (brown).
- (B) *SPARCL1*-transduced CSC-derived tumors show a significantly increased frequency of Iba1<sup>POS</sup> macrophages/microglial cells (brown) as compared to controls. Scale bar: 100 $\mu$ m.
- (C) Quantification of Iba1<sup>POS</sup> cell number in TC and TP after *SPARCL1* overexpression (400x field).
- (D) More Iba1<sup>POS</sup> cells are endowed with features of activated microglia in *SPARCL1*-overexpressing tumors than in controls (200x field).
- (E) Pearson correlation analysis between *SPARCL1* expression and immune infiltrate markers. *Iball* and *CD11b* are total TAM-associated markers; *CD163* and *iNOS* are M2-associated markers.

**Fig. 5 - Advanced MR imaging identifies increased angiogenesis and infiltration in *SPARCL1*-overexpressing PN CSC-derived xenografts.**

- (A) Vessel density and area are significantly increased in xenografts derived from the intracranial implantation of L0605 *SPARCL1*-overexpressing CSCs in nude rats (80 days after transplant).
- (B) *SPARCL1*-overexpressing tumors are endowed with increased contrast enhancement (Post-Gd T1-w images, white areas, dotted line). (C) DCE perfusion MRI shows enhanced tumor vascularity through quantification of plasma volume ( $v_p$ ; yellow spots, arrowhead).
- (D) Tumor volume as measured by T2-weighted imaging (yellow line) is smaller than the tumor volume segmented on isotropic diffusion maps (blue line).

**Fig. 6 - *SPARCL1* expression in glioma cell lines (GCLs) and mesenchymal CSCs enhances neoangiogenesis and induce invasion.**

- (A) *SPARCL1* overexpression results in the promotion of angiogenesis in both GCL- and MES CSC-derived xenografts (CD31, brown; PDGFR $\beta$ , brown) ( $n=3$  mice for each cell line/condition). Scale bar: 100 $\mu$ m.
- (B) Both vessel density and area are significantly increased by *SPARCL1* overexpression.
- (C) *SPARCL1*-transduced GCL/MES CSC-derived tumors show a significantly increased recruitment of Iba1<sup>POS</sup> macrophages/microglial cells (brown) as compared to controls. Scale bar: 100 $\mu$ m.
- (D) Quantification of Iba1<sup>POS</sup> cell number in TC and TP after *SPARCL1* overexpression.
- (E) *SPARCL1* overexpression in GCLs/MES CSCs promotes the local infiltration of tumor cells at the tumor boundary (H&E). White arrows point to neoangiogenic vessels in *SPARCL1*-transduced GCL/MES CSC-derived tumors. Scale bar: 100 $\mu$ m.

**Fig. 7 - *SPARCL1*-induced neoangiogenesis is not primarily mediated by microglia.**

- (A) Treatment of *SPARCL1*-transduced GCL/MES CSC-derived tumors with GW2580 and PLX3397 results in significant decrease in Iba1<sup>POS</sup> macrophages/microglial cells (brown) as compared to

*SPARCL1*-transduced GCL/MES CSC-derived tumors treated with control chow (upper panels).

Angiogenesis is only slightly affected by microglia depletion (CD31, brown).

(B) Quantification of Iba1<sup>pos</sup> cells, vessel density and vessel area in the same tumors.

Journal Pre-proof

**Authors' contributions**

Conceptualization, F.G. and R.G.; Methodology, F.G., R.R., M. B., A.C., and R.G.; Investigation, F.G., A.N., A.L.G, V.P., S.M., M.C., S.R., Mi.C., G.B., L.A., L.S.P., M. B., A.C., P.L.P., R.G.; Formal Analysis, F.G., A.N., A.L.G, V.P., R.R., R.G.; Resources, A.F., P.M.; Writing – Original Draft, F. G. and R.G.; Writing – Review & Editing, F. G., A.N., A.L.G, V.P., R.R., A.C., P.L.P., R.G.; Visualization, R.G.; Supervision, R.G.; Project Administration, R.G.; Funding Acquisition, R.G.

Journal Pre-proof

- Cancer stem cell-derived models do not mimic all the histopathological features of GBM
- There is a strong need for GBM models that reproduce tissue invasion and neoangiogenesis
- *SPARCL1* expression in GBM CSCs promotes brain infiltration and vascular proliferation
- An easy-to-use GBM xenograft model is now available to inform patient-tailored treatment

Journal Pre-proof

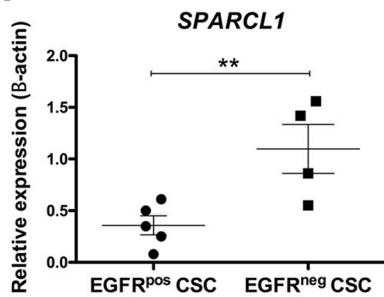
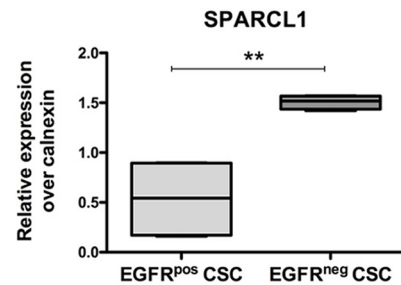
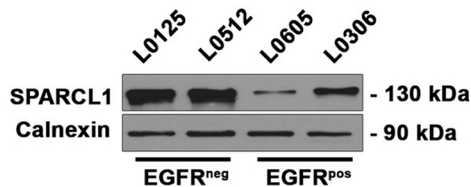
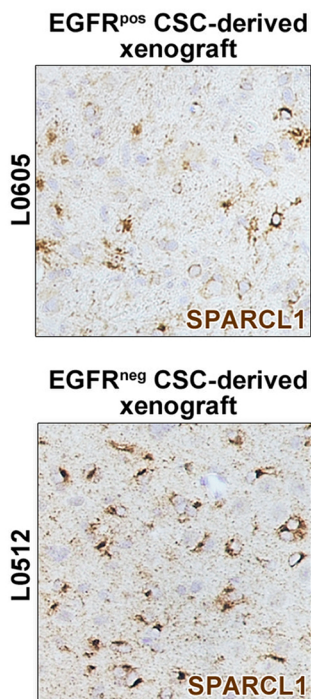
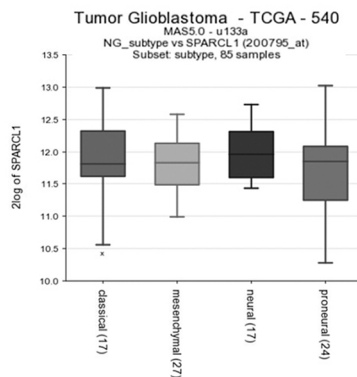
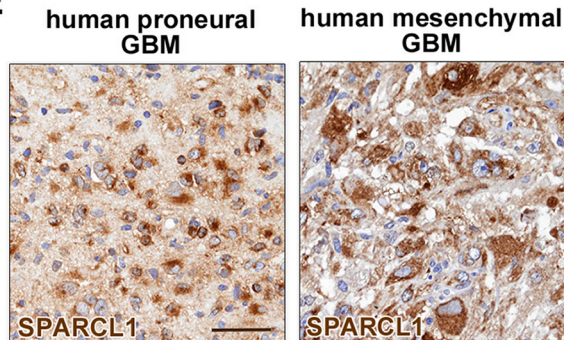
**A****B****C****D****E**

Figure 1

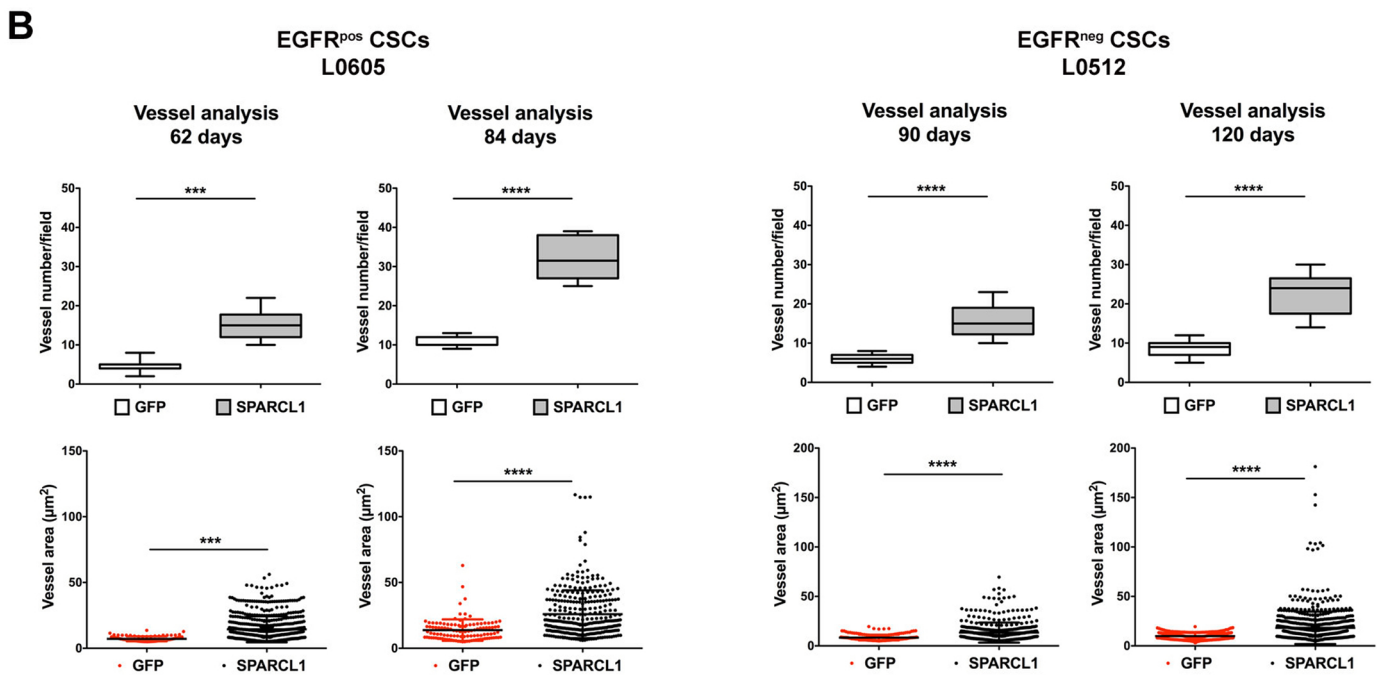
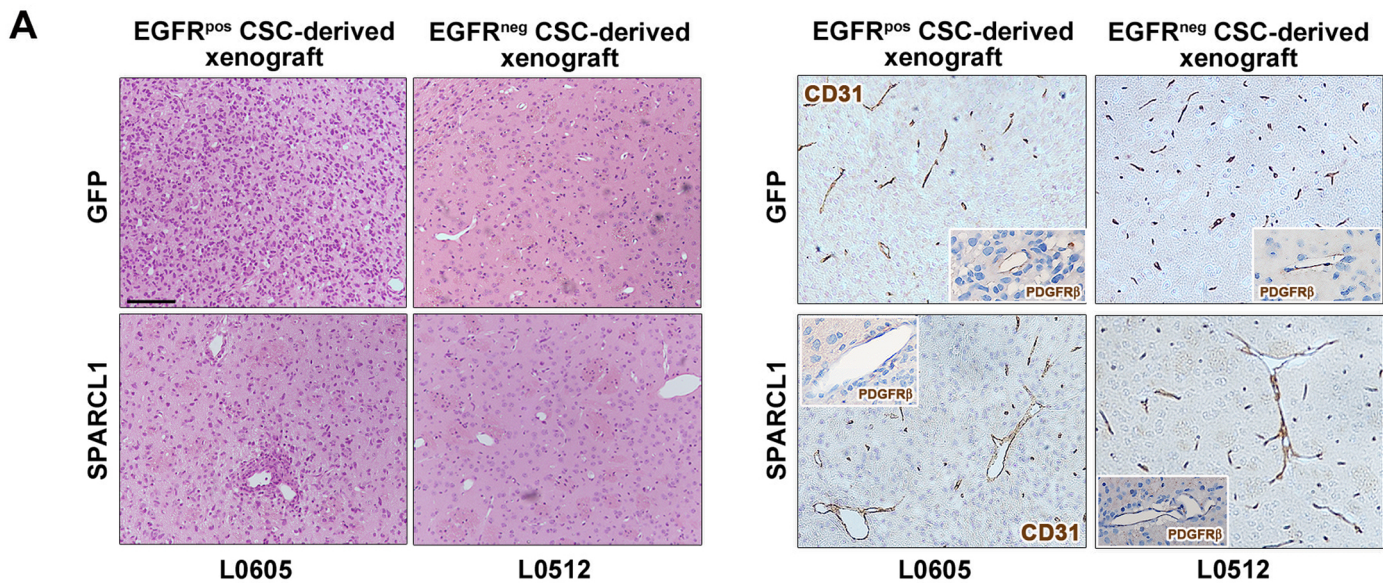


Figure 2

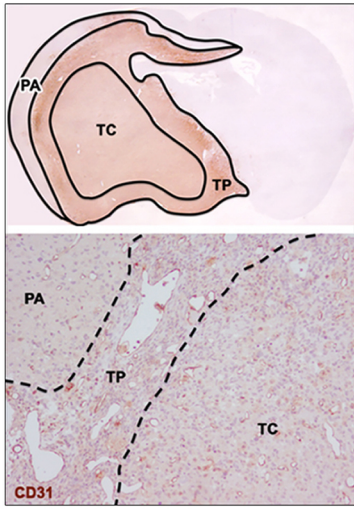
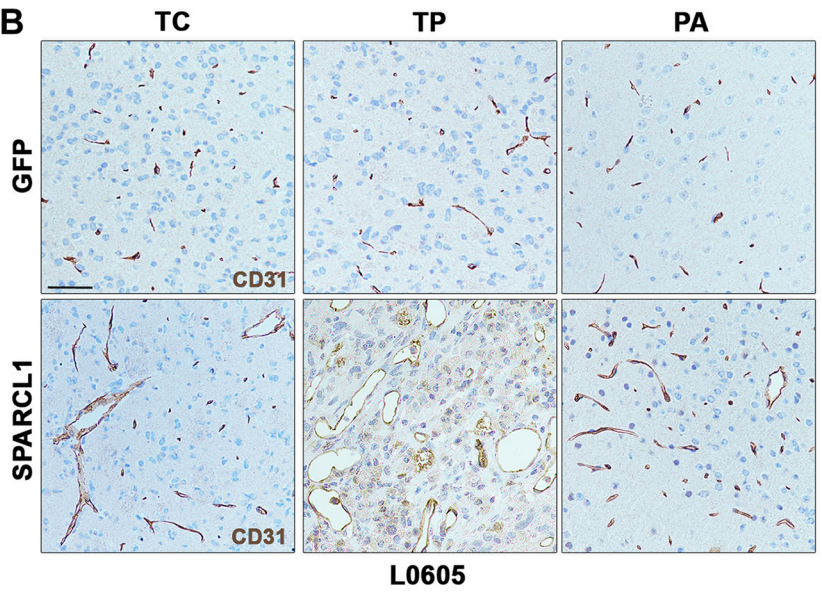
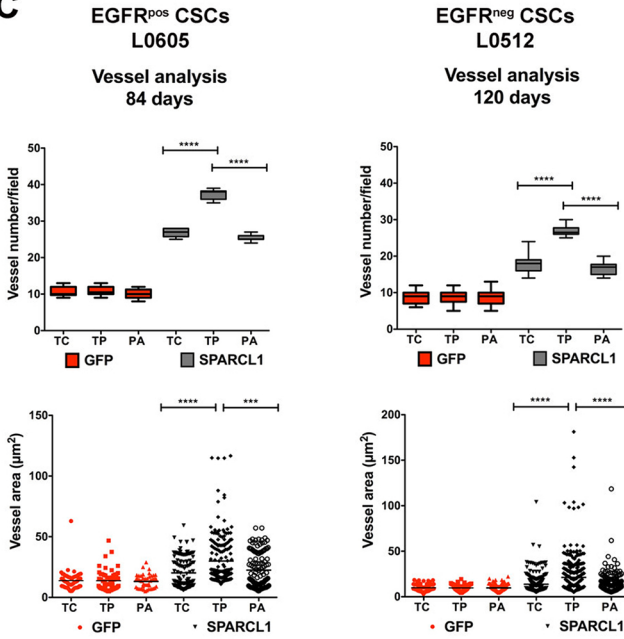
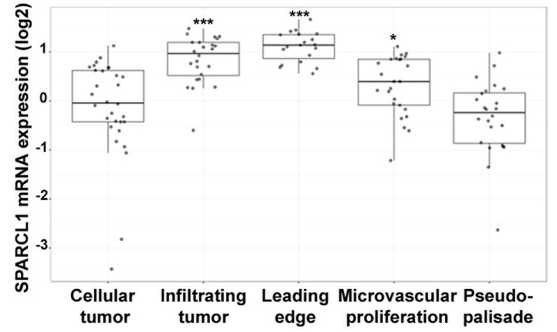
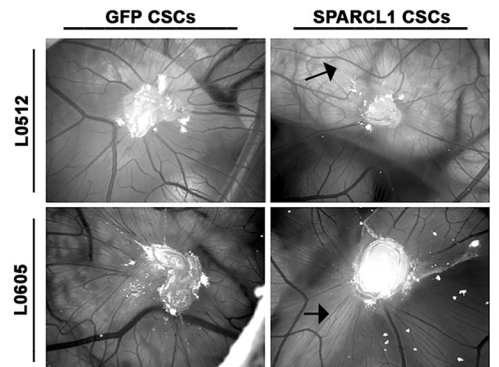
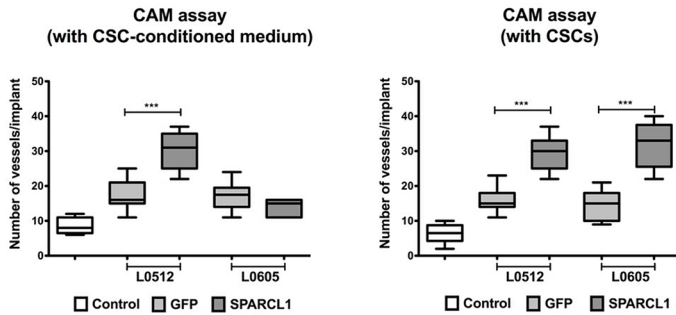
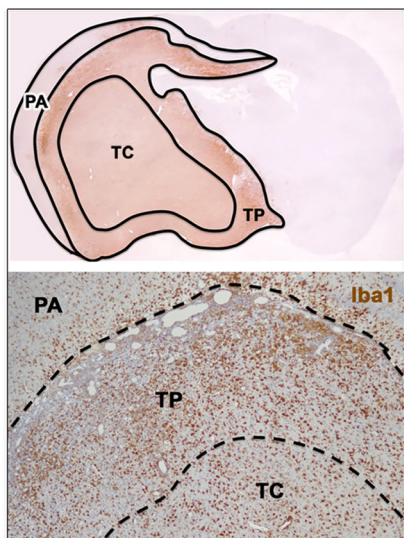
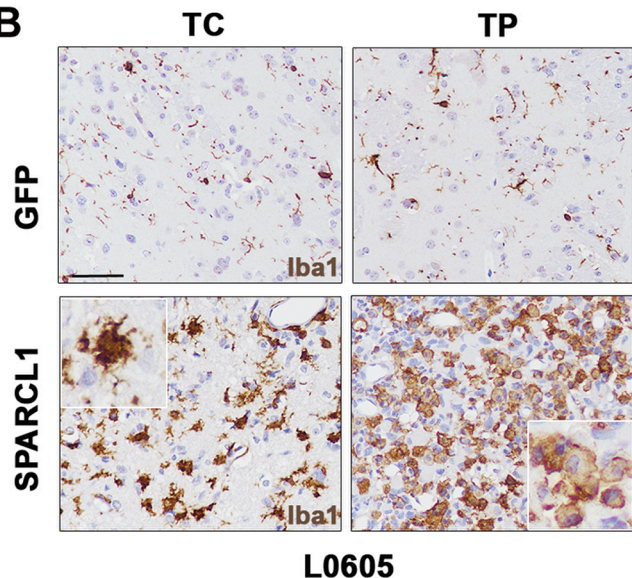
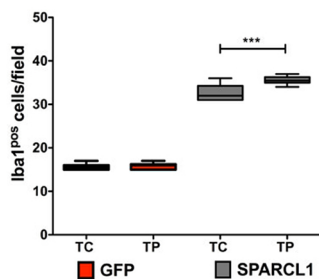
**A****B****C****D****F**

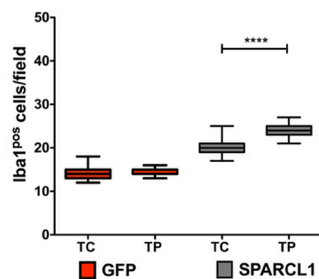
Figure 3

**A****B****C**

**EGFR<sup>pos</sup> CSCs**  
**L0605**  
**Infiltrate analysis**  
**84 days**



**EGFR<sup>neg</sup> CSCs**  
**L0512**  
**Infiltrate analysis**  
**120 days**

**D**

**EGFR<sup>pos</sup> CSCs** **EGFR<sup>neg</sup> CSCs**  
**L0605** **L0512**  
**Infiltrate analysis** **Infiltrate analysis**  
**84 days** **120 days**  
**Activated microglia**

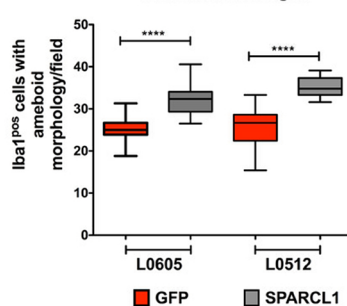
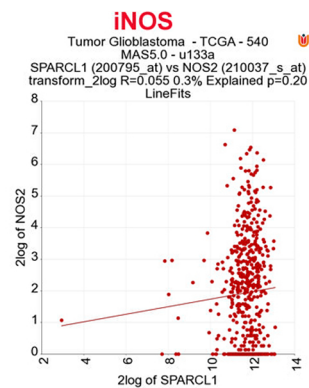
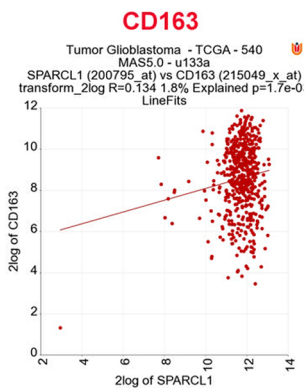
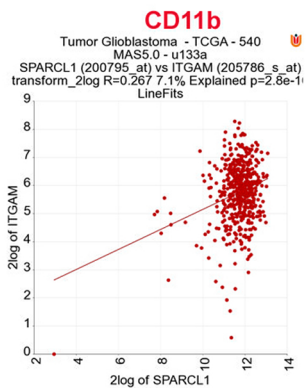
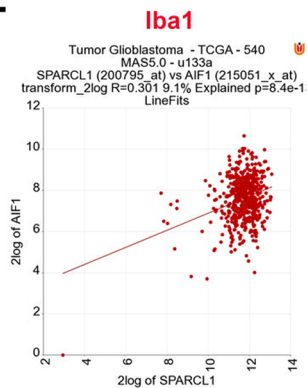
**E**

Figure 4

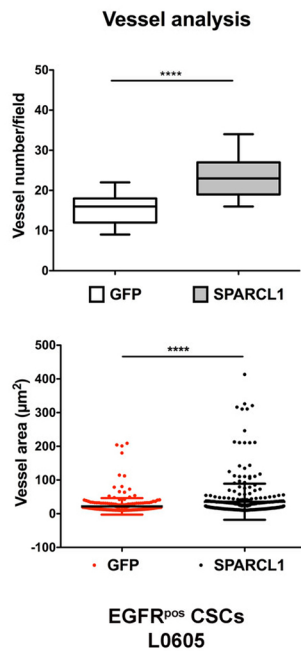
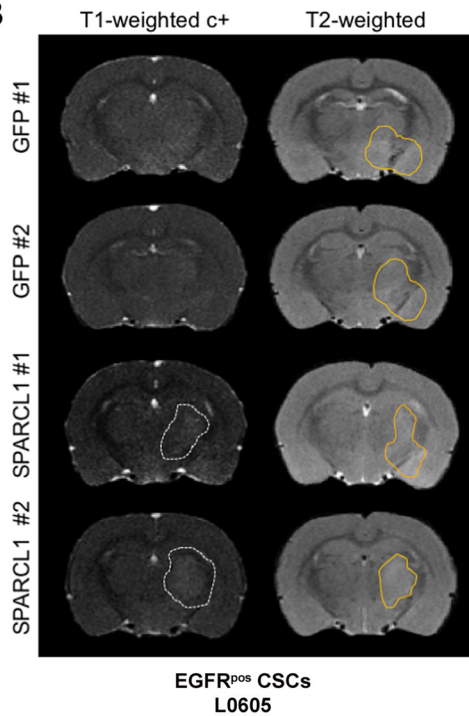
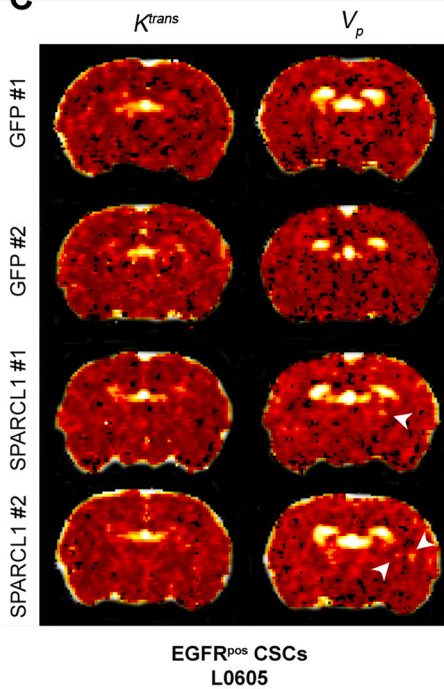
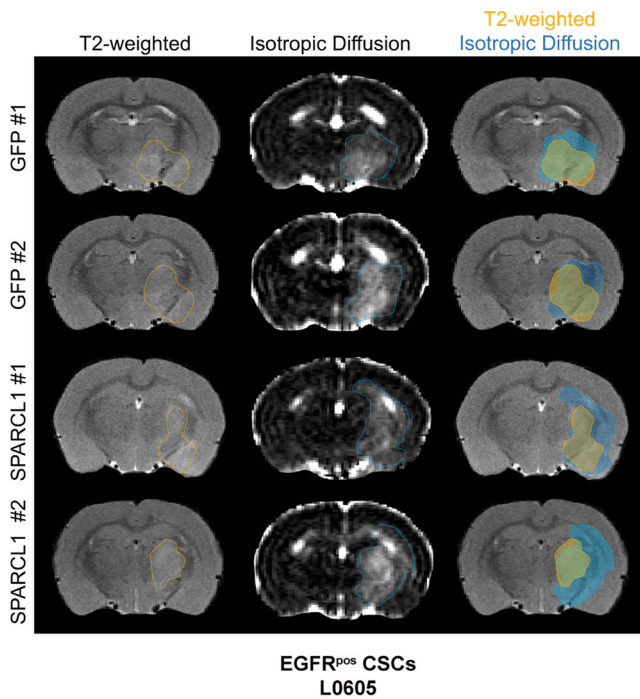
**A****B****C****D**

Figure 5

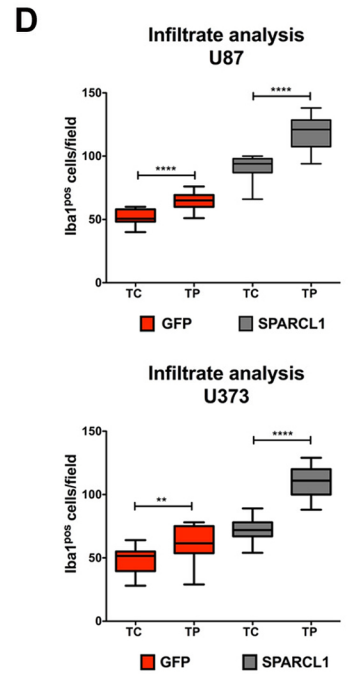
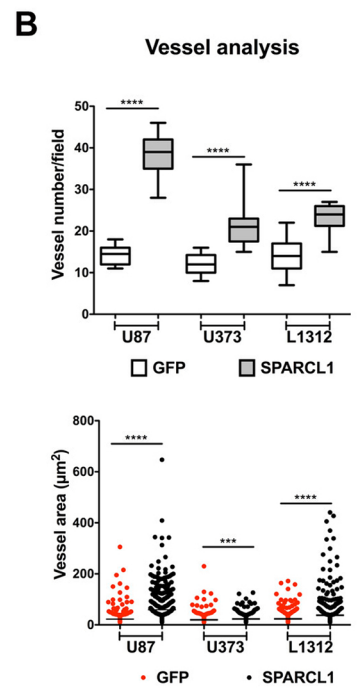
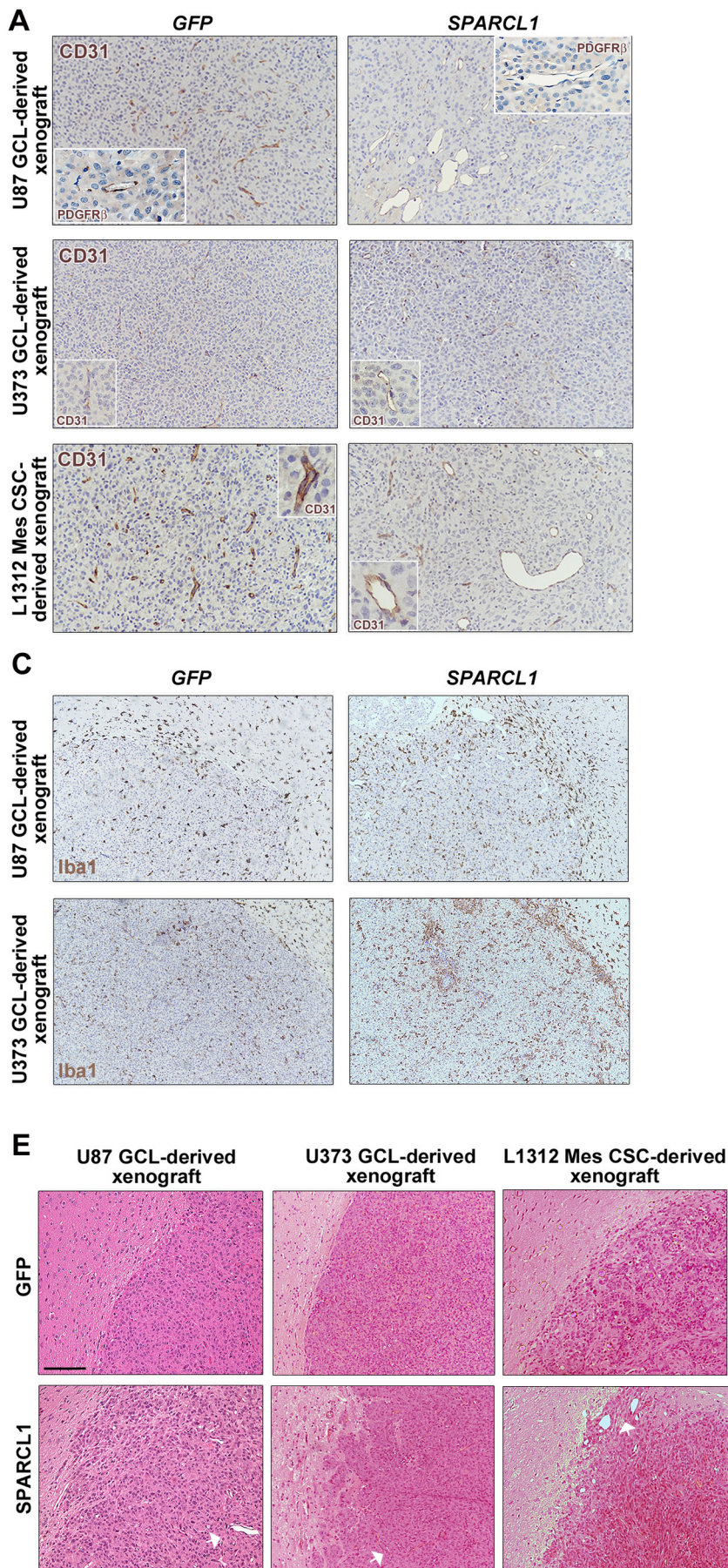


Figure 6

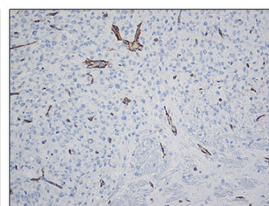
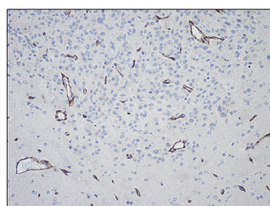
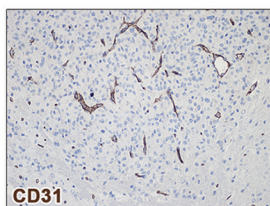
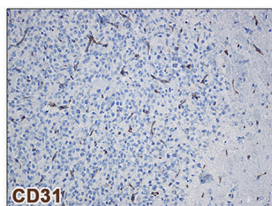
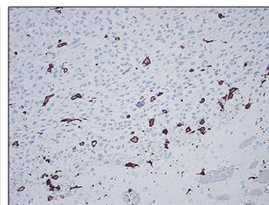
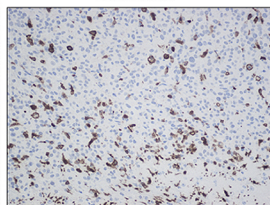
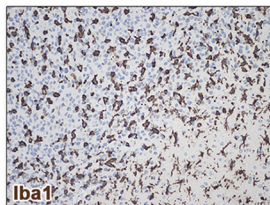
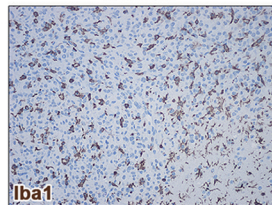
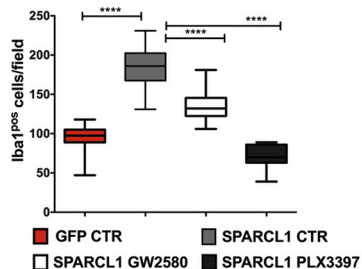
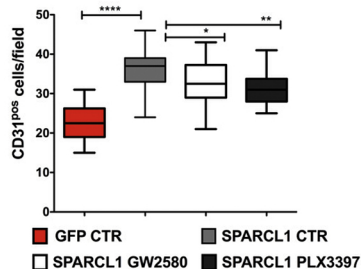
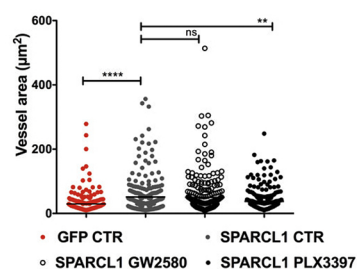
**A****GFP****SPARCL1****Control****Control****GW2580****PLX3397****U87 GCL-derived xenografts****B****Infiltrate analysis  
U87****Vessel analysis  
U87****Vessel analysis  
U87**

Figure 7